Powder Flow Testing with Biaxial and Triaxial devices

C. T. David, R. García-Rojo, H. J. Herrmann, S. Luding (*)
Institute of Computer Physics, Univ. of Stuttgart, Pfaffenwaldring, 27, 70569 Stuttgart, Germany
(*) Particle Technology, Nanostructured Materials, DelftChemTech, TUDelft, Julianalaan 136, 2628 BL Delft, The Netherlands, e-mail: s.luding@tudelft.nl

ABSTRACT

The mechanical response of grains under quasi-static cyclic loading is studied by means of two- and three-dimensional Molecular Dynamics (also called discrete element method). The response of the system is characterized by elastic behavior, softening, plastic yield and critical state flow. Yield is reached for some deformation, and when the contact friction is stronger plastic yield is reached for larger deformation amplitude. In the case of no yield, after many cycles of deformation, accumulation of irreversible plastic strain with the number of cycles is found. For the deviatoric stress and strain, a quasi-periodic ratchet-like behavior is observed. Simulations with different coefficients of friction show weaker plastic strain accumulation in the presence of stronger friction.

KEYWORDS: Particle simulation, friction, ratcheting, creep, strain accumulation

I. INTRODUCTION

The plastic behavior of powder or soil samples depends on the applied strain and on the history of the material [9]. Hysteretic behavior under repeated, cyclic loading is in fact a very relevant characteristic of granular materials. The extensive use of non-cohesive, dry granular materials in foundations of buildings and as roadbeds indicates the urge for developing more efficient methods to study and understand the effects caused by cyclic loading.
Elementary tests are a straightforward way to determine empirical laws and to calculate relevant parameters in constitutive laws. One possibility to perform these experiments is the bi- and tri-axial setup, where the system is subjected to slow, quasi-static deformations, different in two or three directions, respectively. These can be performed periodically, over many cycles. Such tests are usually carried out in order to investigate the elasto-plastic response of granular materials under repeated deformation. An alternative to experiments is the simulation of the system using the discrete elements method (DEM), where the trajectory of individual grains is obtained by the calculation of the interaction forces between particles and integrating the equations of motion [1]. In the simplest case visco-elastic rules can be imposed at each contact, different for the normal and the tangential direction [7,8], but also plastic deformations, cohesion and Coulomb friction are implemented in more advanced models.
When materials accumulate strain in every cycle, their behavior is called ratcheting – if the strain accumulation stops after several cycles, the behavior is called shake-down. The concept of ratcheting was introduced in soil mechanics in order to describe the gradual accumulation of a small permanent deformation [6]. Ratcheting is however a much general concept that has also been studied, driven by the need of understanding steel behavior [4] or biophysical systems such as molecular motors [3]. In a 2D granular packing of discs, subjected to stress controlled cyclic loading, strain accumulations were identified as shakedown, or ratcheting, depending on the amplitude of the stress variations. This particular phenomenon has been intensively investigated in 2D [2,5] and more recently also in 3D [10].

II. MODEL

The elementary units of granular materials, the "mesoscopic" particles, deform locally under stress at the contact point. The realistic modeling of this deformation would be computationally very expensive. Thus the interaction force is related to the overlap of two particles. As a further simplification, these two particles interact only if they are in contact (short range forces), and the force between them is decomposed into a normal and a tangential part.
The *normal force* is, in the simplest case, a linear spring that takes care of repulsion, and a linear dashpot that accounts for dissipation during contact.

$$f_i^n = k\delta + \gamma_0 \dot{\delta}, \tag{1}$$

with spring constant *k* and some damping coefficient γ_0. The half period of a vibration around the equilibrium position can be computed, and one obtains a typical contact duration (response time) $t_c = \pi/\omega$, with $\omega = \sqrt{(k/m_{ij}) - \eta_0^2}$, the eigenfrequency of the contact, the reduced mass $m_{ij} = m_i m_j/(m_i + m_j)$, and the rescaled damping coefficient $\eta_0 = \gamma_0/(2m_{ij})$. The energy dissipation during a collision, as caused by the dashpot is quantified by the restitution coefficent $r = -v_n'/v_n = \exp(-\eta_0 t_c)$, where the prime denotes the normal velocity after a collision.
The *tangential force* involves dissipation due to Coulomb friction, but also some tangential elasticity that allows for stick-slip behavior on the contact level (Luding, 2004). In the static case, the tangential force is coupled to the normal force, Eq. (1), via Coulomb's law, i.e. $f^t \le \mu_s f^n$, where for the limit sliding case one has the dynamic friction with $f^t = \mu_d f^n$. The dynamic and the static friction coefficients follow, in general, the relation $\mu_d \le \mu_s$. However, for the following

simulations, we will apply $\mu = \mu_d = \mu_s$. The static case requires an elastic spring in order to allow for a restoring force, i.e., a non-zero remaining tangential force in static equilibrium due to activated Coulomb friction.

If a contact exists with non-zero normal force, the tangential force can be active too, and we project the corresponding tangential spring into the actual tangential plane. This is necessary, since the frame of reference of the contact may have slightly rotated since the last time-step. $\vec{\xi} = \vec{\xi}' - \hat{n}(\hat{n} \cdot \vec{\xi}')$, where $\vec{\xi}'$ is the old spring from the last iteration, and $\hat{n}$ is the normal unit vector. This action is relevant only for an already existing spring; if the spring is new, the tangential spring-length is zero, but its change is well defined for the next time-interval. The tangential velocity is $\vec{v}_t = \vec{v}_{ij} - \hat{n}(\hat{n} \cdot \vec{v}_{ij})$, with the total relative velocity of the contact surfaces of the particles (*i*,*j*):

$$\vec{v}_{ij} = \vec{v}_i - \vec{v}_j + a_i \hat{n} \times \vec{\omega}_i + a_j \hat{n} \times \vec{\omega}_j \ . \tag{2}$$

Next, we calculate the tangential test-force as the sum of the tangential spring and a tangential viscous force (in analogy to the normal viscous force):

$$\vec{f}_0^t = -k_t \vec{\xi} - \gamma_t \vec{v}_t \ , \tag{3}$$

with the tangential spring stiffness k_t and a tangential dissipation parameter γ_t. As long as $\left|\vec{f}_0^t\right| \le f_C^s$, with $f_C^s = \mu_s f^n$, one has *static friction* and, on the other hand, if $\left|\vec{f}_0^t\right| > f_C^s$, sliding, *dynamic friction* becomes active, with $f_C^d = \mu_d f^n$. Sliding is active as long as $\left|\vec{f}_0^t\right| > \mu_d f^n$, and is changed to sticking only as soon as $\left|\vec{f}_0^t\right| \le f_C^d$ is reached. The corresponding states (static or dynamic) are kept in memory, to be used in the following time-step – and for contact statistics.

In the *static case*, the tangential spring is incremented, $\vec{\xi}' = \vec{\xi} + \vec{v}_t \Delta t_{MD}$, with the time step Δt_{MD} of the DEM simulation, to be used in the next iteration, and the tangential force, Eq. (3), is used.

In the latter, *sliding case*, the tangential spring is adjusted to a length, which is consistent with Coulombs condition

$$\vec{\xi}' = -(1/k_t)\left(f_C^d \hat{t} + \gamma_t \vec{v}_t\right) \ , \tag{4}$$

with the tangential unit vector, $\hat{t} = \vec{f}_0^t \big/ \left|\vec{f}_0^t\right|$, defined by the direction of the tangential test force above, and thus the magnitude of the sliding Coulomb force is used. Inserting the new spring length into Eq. (3) leads to $f_0^t \approx f_C^d$. Note that $\vec{f}_0^t$ and $\vec{v}_t$ are not necessarily parallel in three dimensions.

If all forces are known, acting on a selected particle (either from other particles, boundaries or external forces like gravity or a background damping $\vec{f}_i^b = -\gamma_b \vec{v}_i$), the problem is reduced to the integration of Newton's equations of motion for the translational and rotational degrees of freedom:

$$m_i \frac{\mathrm{d}^2}{\mathrm{d}t^2} \vec{r}_i = \vec{f}_i + m_i \vec{g} \quad \text{and} \quad I_i \frac{\mathrm{d}}{\mathrm{d}t} \vec{\omega}_i = \vec{t}_i \ , \tag{5}$$

with the gravitational acceleration $\vec{g}$, the mass m_i of the particle, its position $\vec{r}_i$, the total force $\vec{f}_i = \sum_c \vec{f}_i^c$, acting on it due to contacts with other particles or with the walls, its moment of inertia I_i, its angular velocity $\vec{\omega}_i$, and the total torque $\vec{t}_i = \sum_c \vec{l}_i^c \times \vec{f}_i^c$, with the center-contact "branch" vector $\vec{l}_i^c$.

In our DEM simulations, a three-dimensional triaxial box is used. The walls are either fixed or stress controlled. Typical values of the test include a confining stress p_0=1 kN/m^2, a wall-mass m_w=2 kg, and a viscosity of the wall, γ_w=200 kg/s, which corresponds to a viscous relaxation time t_w=0.01 s.

For the initial preparation of the sample, the spheres (with radii randomly drawn from a Gaussian distribution centered at 5 mm, a minimum of 3 mm and a standard deviation of 0.7 mm) were

placed on a square lattice (big enough for them not to overlap). Then the box is compressed by imposing a confining pressure, p_0, in order to achieve a homogeneous, isotropic initial condition. Inhomogeneities in the distribution of large and small particles were observed when the compression was performed too fast and only from one side. The simulations presented below were compressed from all sides at the same time to avoid this effect. The preparation stage is finished when the kinetic energy becomes much smaller than the potential energy stored in the contacts. A periodic loading with period t_0 is applied next through a side of the box, while keeping the other stresses constant. The fact that all walls are stress controlled allows for a moving center of mass of the system. A more detailed study involving alternative boundary conditions is in progress.

III. RESULTS AND DISCUSSION

Different friction coefficients and numbers of particles have been investigated in 2d and 3d: In both dimensions, the particles are assumed to be spherical with density ρ=2000 kg/m^3, which leads to a mass m=1 g for a sphere with the (mean) radius a=5 mm. The normal and tangential spring constants used (as described in the previous section) are in 3D: k_n=5000 N/m, and k_t/k_n=0.2. The damping coefficients applied were: γ_0=0.05 kg/s, γ_t=0.01 kg/s, γ_b=0.2 kg/s, γ_{br}=0.05 kg/s, the latter two corresponding to background translational and rotational damping, respectively. This leads to a typical contact duration, t_c=10^{-3} s, a restitution coefficient, r=0.95, and background damping relaxation time, t_b=0.005 s. The DEM step used is Δt_{MD}=2.10^{-5} s, such that we can be sure that $\Delta t_{MD} << t_c < t_b < t_0$. See Fig. 1 for a snapshot of typical systems in 2d and 3d.

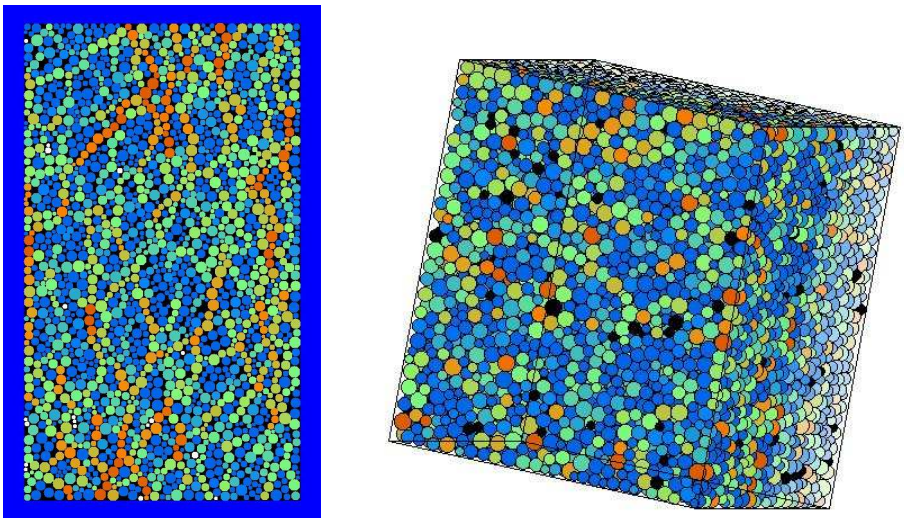

Figure 1: Snapshot of the model systems in 2d (left) with N=1950 particles, see [7,8] for details, and in 3d (right) with N=20000 particles. The color code blue/green/red indicates particles feeling weak/medium/strong forces.

Deformation modes

Deformations can be applied either directly, by controlling strain, or indirectly by controlling/varying stress. The former approach was used in Refs. [7,8] for 2D samples, see Fig. 2 (left), so that the latter is discussed here for the 3D case, see Fig. 2 (right). The horizontal stress on a cuboid packing of 3375 spheres is modified with an amplitude $\Delta\sigma = 0.2 p_0$, such that $2\sigma_{xx} := \sigma_{xx}^{left} + \sigma_{xx}^{right}$, and $2\sigma_{xx} = 2p_0 + \Delta\sigma[1-\cos(2\pi t/t_0)]$, where t is the time and t_0=10 s is the period of the cyclic loading. We performed also simulations with periods t_0=20 s and 40 s, and obtained no significant differences. The deviatoric stress $\sigma_D = 2(\sigma_{xx} - \sigma_{yy})/3$ is plotted against the

deviatoric strain $\varepsilon_D = \varepsilon_{xx} - \varepsilon_{yy}$, in Fig. 2, with $\varepsilon_{xx} = 1 - L_x / L_x^0$ and $\varepsilon_{yy} = 1 - L_y / L_y^0$, where the L are the system sizes in directions x, y, and z, and the zero superscript indicates the original value before stress is changed.

The stress-strain relation consists of the initial, linear elastic part starting from the origin. For the strain-controlled case (large amplitude), the stress increases, reaches a maximum (with zero slope) and decreases down to the critical state flow level. The macroscopic effective friction is for peak and for critical state flow is plotted in Fig. 3 (left). Note that it is not directly correlated with the microscopic friction coefficient. The peak friction depends on the initial conditions, whereas the critical state friction does not; the former saturates well above μ=1, while the latter already saturates at μ =0.4.

For the stress-controlled case (small amplitude), the maximum is not reached after one cycle. When stress is decreased and increased again, open hysteresis loops develop. The accumulated strain is maximal for the first cycle and then becomes smaller with each cycle until an approximately constant rate of accumulation is reached, see Fig. 3 (right). The stronger the microscopic contact friction, the smaller the rate of strain accumulation. For large enough friction, above a certain threshold, shakedown is evidenced, i.e., strain is not accumulated anymore.

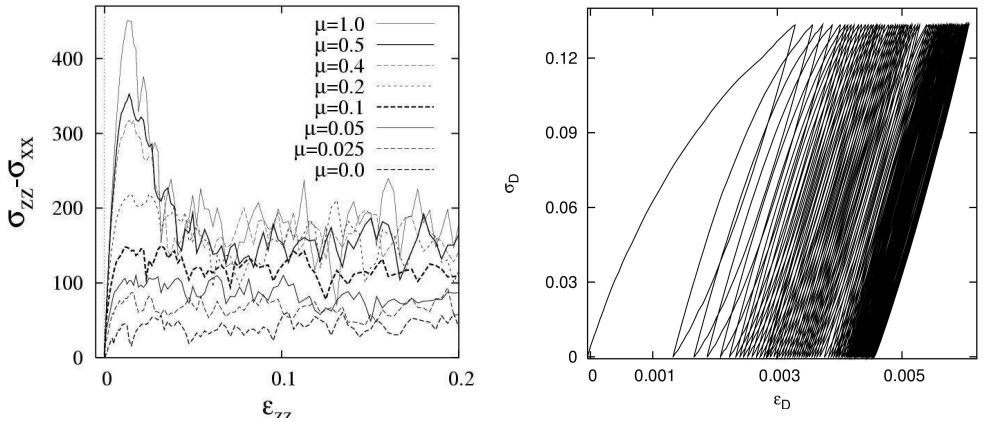

Figure 2: (Left) Deviatoric stress versus vertical strain (in 2D) for a strain controlled deformation test – with continuously increasing vertical strain – for different coefficients of friction as given in the inset, when the horizontal stress is fixed to σ_{xx}=200. (Right) Deviatoric stress plotted against deviatoric strain (in 3D) during the first 100 cycles of stress controlled deformation (as described in the text) for a sample of N=3375 spheres.

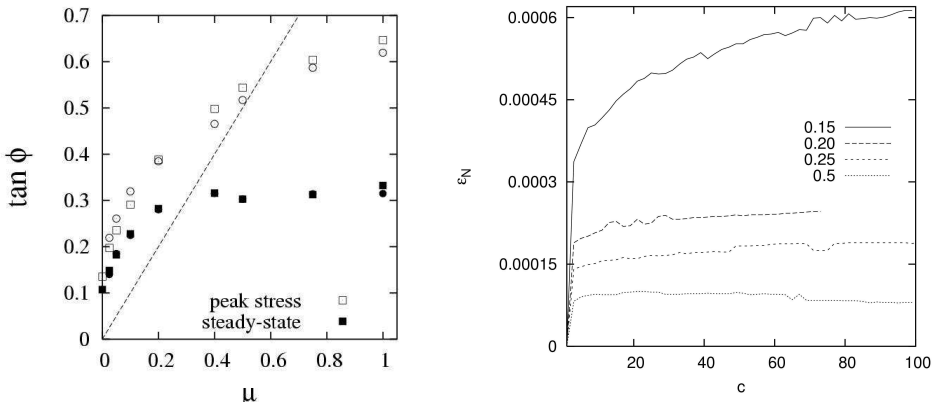

Figure 3: (Left) Macroscopic friction coefficient at peak (open symbols) and at critical state flow (solid symbols) plotted as function of the microscopic friction coefficient. The different symbols (circles and squares) correspond to different initial conditions. (Right) Strain accumulation as a function of the number of cycles, c, for different microscopic friction coefficients as given in the inset.

IV. DISCUSSION AND CONCLUSIONS

In summary, yield and critical state flow was reported from 2d simulations, while shakedown and ratcheting was observed in 3d model granulates, both consisting of polydisperse, frictional spheres. From our results we conclude that the yield limit and the internal, macroscopic friction, as well as the boundary between shakedown and ratcheting depends on friction in a non-trivial way. The stronger the contact friction, the larger the peak stress and also the critical state stress in 2d. The former increases stronger, however, and also depends on the initial conditions; the latter increases rapidly and saturates at moderate contact friction and, furthermore, does not depend on the initial situation. For the chosen small stress changes in 3d, ratcheting is only observed for rather weak friction, while stronger friction seems to work against ratcheting by stabilizing the packing due to the stronger tangential forces.
The present study is only the first step towards a more detailed exploration of the influence of various other material- and system-parameters, involving variations of the strain and stress amplitudes, of the friction modesl, boundary conditions, and others.

V. ACKNOWLEDGEMENTS

The authors acknowledge support from the EU project Degradation and Instabilities of Geomaterials with Application to Hazard Mitigation (DIGA) in the framework of the Human Potential Program, Research Training Networks (HPRN-CT-2002-00220), the Deutsche Forschungsgemeinschaft (DFG), and FOM (Fundamenteel Onderzoek der Materie), financially supported by the Nederlandse Organisatie voor Wetenschappelijk Onderzoek (NWO).

VI. REFERENCES

[1] Allen, M., P. Tildesley (1987). *Computer Simulation of Liquids.* Oxford: Oxford University Press.

[2] Alonso-Marroquin F. and H. J. Herrmann (2004). *Ratcheting of granular materials*, Phys. Rev. Lett. 92, 054301 (2004).

[3] Astumian, R. (2001). *Making molecules into motors*, Scientific American 58, 57-64.

[4] Colak, O. U. and E. Krempl (2003). *Modelling of uniaxial and biaxial ratcheting behavior of 1026 Carbon steel using the simplified Viscoplasticity Theory Based on Overstress*, Acta Mechanica (New York) 160, 27-44.

[5] García-Rojo, R. and H. J. Herrmann (2005). *Shakedown of unbound granular material*, Granular Matter 7(2), in press.

[6] Lekarp, F., U. Isacsson and Dawson A (2000). *Permanent strain response of unbound aggregates*, J. Transp. Engng.-ASCE 126 (1). 66-83.

[7] Luding, S. (2004), *Micro-macro transition for anisotropic, frictional granular packings*. Int. J. Sol. Struct. 41, 5821-5836.

[8] Luding S. (2004b), *Molecular dynamics simulations of granular materials*. In H. Hinrichsen and D. E. Wolf (Eds.), The Physics of Granular Media, Wiley VCH, Weinheim, Germany, pp 299-324.

[9] Vanel, L., D Howell, D. Clark, R.P. Behringer and E. Clement (1999), *Effects on construction history on the stress distribution under a sand pile*, Physical Review E 60, 5.

[10] C. T. David, R. Garcia Rojo, H. J. Herrmann, and S. Luding, *Hysteresis and creep in powders and grains* , in: Powders and Grains 2005, Stuttgart, July 2005, R. Garcia-Rojo, H. J. Herrmann, and S. McNamara (Eds.), Balkema, Leiden, Netherlands, pp. 291-294